Modelling carbon nanotube based biosensor

**Romas Baronas · Juozas Kulys ·
Karolis Petrauskas · Julija Razumiene**

Abstract   This paper presents a two-dimensional-in-space mathematical model of
an amperometric biosensor based on an enzyme-loaded carbon nanotubes layer
deposited on a perforated membrane. The developed model is based on non-
linear non-stationary reaction-diffusion equations. By changing input parameters the
output results are numerically analysed with a special emphasis to the influence of
the geometry and the catalytic activity of the biosensor to its response. The numerical
simulation at transition and steady state conditions was carried out using the finite
difference technique. The mathematical model and the numerical solution were val-
idated by experimental data. The obtained agreement between the simulation results
and experimental data was admissible at different concentrations of the substrate and
the mediator.

1 Introduction

Biosensors are analytical devices mainly used to measure concentrations of analytes.
Main parts composing a biosensor are a biologically active element, usually an enzyme,

R. Baronas · K. Petrauskas (✉)
Faculty of Mathematics and Informatics, Vilnius University, Naugarduko 24,
03225 Vilnius, Lithuania
e-mail: k.petrauskas@gmail.com

J. Kulys
Department of Chemistry and Bioengineering, Vilnius Gediminas Technical University,
Sauletekio Ave. 11, 10223 Vilnius, Lithuania

J. Razumiene
Department of Bioanalysis, Institute of Biochemistry, Vilnius University, Mokslininku 12,
08662 Vilnius, Lithuania

that recognizes a specific analyte (substrate) and a transducer that converts biological recognition event into an electrical signal [1,2]. Amperometric biosensors measure a current arising on the electrode because of the direct electrochemical reduction or oxidation of the biochemical reaction product. The current collected by the transducer is usually proportional to the concentration of the analyte. Amperometric biosensors are relatively cheap, highly sensitive and reliable devices, widely used in clinical diagnostics, drug detection, food analysis and environment monitoring [3–5].

Since carbon nanotubes (CNT) were discovered [6], they were used in various applications because of their unique structural and electronic properties. Multi (MWCNT) as well as single (SWCNT) walled carbon nanotubes emerged as a promise component for developing novel biosensors of the extraordinary sensitivity [7–11]. Recently, an innovative approach in design of biosensors based on CNT layer deposited on the polycarbonate perforated membrane has been proposed [12].

To improve an efficiency of the development of novel biosensors and to optimise their configuration a model of the real biosensor should be built [13,14]. Starting from the seventies various mathematical models have been successfully used as important tools to study and optimize analytical characteristics of actual biosensors [15–17]. A comprehensive review on the modelling of the amperometric biosensors has been presented by Schulmeister [18] and more recently by Baronas et al. [19].

To solve the problems currently limiting the practical use of CNT-based biosensors, the mass transport and the enzyme kinetics within the biosensors have to be comprehensively investigated [20]. Recently, a two-compartment mathematical model describing the transport and the kinetics of the substrate and the mediator within chemically modified electrodes comprising of redox enzymes immobilised in CNT meshes dispersed on support electrode surfaces has been developed by Lyons [20,21]. The one-dimensional-in-space boundary value problem was solved analytically assuming the steady state conditions. Practical biosensors are usually covered by outer porous or perforated membranes [7–12]. The outer membrane increases the biosensor stability and prolongs its calibration curve [1,2,22].

This paper presents a two-dimensional-in-space mathematical model of an amperometric biosensor based on an enzyme loaded CNT layer and a perforated membrane [12]. The holes in perforated membrane are partially filled with the carbon nanotubes. The developed model is based on non-stationary non-linear reaction-diffusion equations [19,23]. It involves the following regions: the enzyme and the CNT layers where enzymatic reactions as well as the mass transport by diffusion take place, a diffusion limiting region where only the mass transport by diffusion takes place and a convective region where the analyte concentration is maintained constant.

By changing input parameters the output results were numerically analysed with a special emphasis to the influence of the geometry and the catalytic activity of the biosensor on the biosensor response. The numerical simulation at transition and steady state conditions was carried out using the finite difference technique [19,23,24]. The mathematical model and the numerical solution were validated by experimental data [12]. The obtained agreement between the simulation results and experimental data was admissible at different concentrations of the substrate and the mediator.

2 Principal structure of the biosensor

Figure 1 shows a schematic representation of the modelling biosensor based on an enzyme-loaded CNT composite electrode and a perforated membrane [12].

The considered biosensor was built by assembling several layers of different materials and sizes. These layers were deposited on the insulating film shown in Fig. 1 as the bottom layer. When preparing the biosensor, single walled CNT layer was deposited on a polycarbonate perforated membrane and loaded with an enzyme. The enzyme was additionally constrained in a relatively thin layer between the insulating film and the CNT layer. The single walled carbon nanotubes form an composite electrode of the biosensor. Due to the technology of the biosensor preparation, some carbon nanotubes were sinked into the holes of the perforated membrane.

In the enzyme-loaded regions, we consider a two-stage scheme of the enzyme (E) catalysed substrate (S) conversion to the product (P) in a presence of the mediator (M),

$$E_{ox} + S \xrightarrow{k_1} E_{red} + P, \tag{1}$$

$$E_{red} + M_{ox} \xrightarrow{k_2} E_{ox} + M_{red}, \tag{2}$$
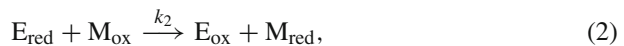
where E_{ox} and E_{red} stand for the oxidised and reduced forms of the enzyme, respectively, while M_{ox} and M_{red} represent the oxidised and reduced forms of the mediator, respectively. In the CNT region, the mediator in the reduced form (M_{red}) is electrochemically re-oxidised and electrons are released forming the output current,

$$M_{red} \xrightarrow{e} M_{ox}. \tag{3}$$

As it is common for the amperometric biosensors, the electrochemical reaction (3) is assumed to be very fast [1,2].

The holes in the perforated membrane were modelled by right cylinders of uniform diameter and spacing, forming a regular hexagonal pattern. For the simplicity, it is reasonable to consider a circle whose area equals to that of the hexagon and to regard one of the cylinders as a unit cell of the biosensor. Due to the symmetry of the unit cell, only a half of the transverse section of the unit cell is considered in the mathematical model formulated in cylindrical coordinates [22]. Very similar approach has been used in modelling of partially blocked electrodes [25,26].
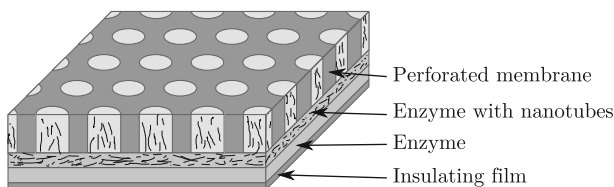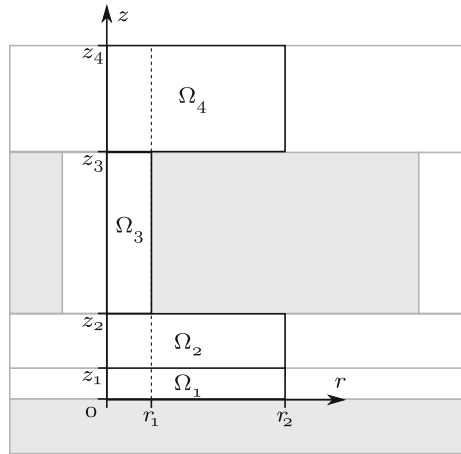

— Perforated membrane
— Enzyme with nanotubes
— Enzyme
— Insulating film

Fig. 1 Principal structure of the biosensor based on an enzyme-loaded CNT composite electrode and a perforated membrane. The figure is not to scale

The profile of the unit cell of the biosensor is shown in Fig. 2. In this figure, r_1 stands for the radius of the holes in the perforated membrane, r_2 is the radius of the unit cell of the biosensor, regions Ω_1 and Ω_2 represent the enzyme and the enzyme-loaded CNT layers, respectively, z_1 is the thickness of the enzyme layer, $z_2 - z_1$ is the thickness of the CNT layer, $z_3 - z_2$—the thickness of the perforated membrane, Ω_3 represents a hole in the perforated membrane, Ω_4 stands for the external diffusion layer of the thickness $z_4 - z_3$.

The analysed substrate gets into the biosensor from the buffer solution through the holes of the perforated membrane. The external diffusion layer Ω_4 can be treated as the Nernst diffusion layer [27]. According to the Nernst approach the layer of the thickness $z_4 - z_3$ remains unchanged with time. It is also assumed that away from it the solution is a uniform in the concentration.

3 Mathematical model

Let Ω_i be the open region presented in Fig. 2, $i = 1, 2, 3, 4$,

$$
\begin{aligned}
\Omega_1 &\equiv (0, r_2) \times (0, z_1), \quad \Omega_2 \equiv (0, r_2) \times (z_1, z_2), \\
\Omega_3 &\equiv (0, r_1) \times (z_2, z_3), \quad \Omega_4 \equiv (0, r_2) \times (z_3, z_4).
\end{aligned}
\tag{4}
$$

Additionally, let $\overline{\Omega}_i$ be the closed region corresponding to the open region Ω_i, $i = 1, 2, 3, 4$. For the further convenience, we introduce the boundaries of the regions:

$$
\Gamma_i = \begin{cases}
[0, r_2] \times \{0\}, & \text{for } i = 0, \\
\overline{\Omega}_i \cap \overline{\Omega}_{i+1}, & \text{for } i = 1, 2, 3, \\
[0, r_2] \times \{z_4\}, & \text{for } i = 4,
\end{cases}
\tag{5}
$$

where Γ_0, Γ_4 stand for the lower and the upper boundaries of the unit cell of the biosensor, and Γ_j denotes the boundary between adjacent regions Ω_j and Ω_{j+1}, $j = 1, 2, 3$.

3.1 Governing equations

The biosensor operation is described by non-linear reaction-diffusion equations [19, 23]. The mathematical model is formulated in a two-dimensional domain in cylindrical coordinates (see Fig. 2). The different diffusion coeficients for each species were chosen in different directions r and z due to anisotropic properties of CNT in bulk and pores [28,29].

To simplify the expression of the governing equations of the model, we introduce an operator Λ to describe the diffusion term in cylindrical coordinates r and z,

$$\Lambda(U) \equiv D_{U,r} \frac{1}{r} \frac{\partial}{\partial r} \left(r \frac{\partial U}{\partial r} \right) + D_{U,z} \frac{\partial^2 U}{\partial z^2}, \tag{6}$$

where U is a concentration of a particular species U, $D_{U,r}$ and $D_{U,z}$ are the diffusion coefficients of the species U in the directions r and z, respectively.

The enzyme in the biosensor is immobilised and therefore is not affected by the diffusion. In the enzyme-loaded regions Ω_1 and Ω_2, the dynamics of the enzyme concentration is affected only by the enzymatic reactions (1) and (2). The dynamics of the enzyme concentration is described by the following reaction equations:

$$\frac{\partial E_{ox,i}}{\partial t} = -k_1 E_{ox,i} S_i + k_2 M_{ox,i} E_{red,i},$$
$$\frac{\partial E_{red,i}}{\partial t} = k_1 E_{ox,i} S_i - k_2 M_{ox,i} E_{red,i}, \quad (r, z) \in \Omega_i, \quad i = 1, 2, \quad t > 0, \tag{7}$$

were t stands for time, $U_i = U_i(r, z, t)$, $U \in \{E_{ox}, E_{red}, S, M_{ox}\}$ is the concentration of the corresponding species in the area $\overline{\Omega}_i$, coefficients k_1 and k_2 are the rates of the reactions (1) and (2), respectively.

The mass transport by diffusion of the substrate takes place in all the regions: the enzyme layer (Ω_1), the enzyme-loaded CNT layer (Ω_2), the holes of the perforated membrane (Ω_3) and the Nernst diffusion layer (Ω_4). In the both layers containing the enzyme, the substrate also participates in the reaction (1). The dynamics of the substrate concentration S_i in the region Ω_i is described as follows ($i = 1, 2, 3, 4$):

$$\frac{\partial S_i}{\partial t} = \begin{cases} \Lambda(S_i) - k_1 E_{ox,i} S_i, & \text{for } i = 1, 2, \\ \Lambda(S_i), & \text{for } i = 3, 4. \end{cases} , \quad (r, z) \in \Omega_i, \ t > 0, \tag{8}$$

The mass transport by diffusion of the oxidised mediator M_{ox} takes place inside the entire biosensor as well as in the outer diffusion layer. In both layers containing the enzyme, the mediator is involved in the enzymatic reaction (2). In the CNT regions, the oxidised mediator is regenerated by the electrochemical reaction (3). The reaction (3) is assumed to be very fast as it is common for amperometric biosensors. The whole mediator in its reduced form (M_{red}) is immediately re-oxidised. Therefore,

whole M_{ox} consumed in the reaction (2) is immediately regenerated in the reaction (3). The immediate regeneration of M_{ox} leads to skipping the reaction terms in the equation describing the dynamics of the concentration $M_{ox, 2}$ in the region Ω_2. Consequently, the dynamics of the M_{ox} in the region Ω_i is described by the following equations $(t > 0)$:

$$\frac{\partial M_{ox, i}}{\partial t} = \begin{cases} \Lambda(M_{ox, i}) - k_2 M_{ox, i} E_{red, i}, & \text{for } i = 1, \\ \Lambda(M_{ox, i}), & \text{for } i = 2, 3, 4, \end{cases} \quad (r, z) \in \Omega_i. \quad (9)$$

The mediator in the reduced form (M_{red}) is generated by the reaction (2). In the enzyme layer (region Ω_1), the M_{red} is only produced. The immediate re-oxidation of the reduced mediator in the reaction (3) leads to zero concentration of M_{red} in the enzyme-loaded CNT layer (region Ω_2). Therefore, the dynamics of the concentration $M_{red,1} = M_{red,1}(r, z, t)$ of the M_{red} is described only in the region Ω_1,

$$\frac{\partial M_{red,1}}{\partial t} = \Lambda(M_{red,1}) + k_2 M_{ox, 1} E_{red,1}, \quad (r, z) \in \Omega_1, \; t > 0. \quad (10)$$

3.2 Boundary conditions

During the modelling experiments the buffer solution is well stirred. This leads to constant concentrations of the species above the Nernst diffusion layer [27],

$$S_4(r, z_4, t) = S_0, \quad M_{ox, 4}(r, z_4, t) = M_0, \quad r \in [0, r_2], \; t > 0, \quad (11)$$

where S_0 and M_0 are the concentrations of the substrate and the mediator in the buffer solution.

The non-leakage boundary conditions are used to represent the symmetry of the unit cell of the biosensor. These conditions are also applied to the surface of the perforated membrane when $t > 0$,

$$\frac{\partial M_{red,1}}{\partial r}\bigg|_{\Pi_1} = 0; \quad \frac{\partial S_i}{\partial n}\bigg|_{\Pi_i} = \frac{\partial M_{ox,i}}{\partial n}\bigg|_{\Pi_i} = 0, \quad i = 1, 2, 3, 4, \quad (12)$$

where n stands for the normal direction, and $\Pi_i = \overline{\Omega}_i \setminus \Omega_i \setminus \Gamma_{i-1} \setminus \Gamma_i$.

The boundary Γ_0 represents the surface of the insulating film where non-leakage conditions are also applied to all the diffusive species,

$$\frac{\partial S_1}{\partial z}\bigg|_{\Gamma_0} = \frac{\partial M_{ox, 1}}{\partial z}\bigg|_{\Gamma_0} = \frac{\partial M_{red,1}}{\partial z}\bigg|_{\Gamma_0} = 0, \quad t > 0. \quad (13)$$

On the boundary between adjacent regions having different diffusivities, we define the matching conditions ($t > 0$),

$$D_{S_i,z} \left.\frac{\partial S_i}{\partial z}\right|_{\Gamma_i} = D_{S_{i+1},z} \left.\frac{\partial S_{i+1}}{\partial z}\right|_{\Gamma_i}, \quad S_i|_{\Gamma_i} = S_{i+1}|_{\Gamma_i}, \quad i = 1, 2, 3, \quad (14)$$

$$D_{M_{ox,i},z} \left.\frac{\partial M_{ox,i}}{\partial z}\right|_{\Gamma_i} = D_{M_{ox,i+1},z} \left.\frac{\partial M_{ox,i+1}}{\partial z}\right|_{\Gamma_i},$$

$$M_{ox,i}\big|_{\Gamma_i} = M_{ox,i+1}\big|_{\Gamma_i}, \quad i = 2, 3. \quad (15)$$

On the boundary Γ_1, where the enzyme-loaded CNT layer (Ω_2) touches the entirely enzyme-loaded layer (Ω_1), the concentration of M_{ox} is influenced by the reaction (3). The mediator re-oxidation reaction (3) is assumed to be so fast, that whole diffusive M_{red} touching the border Γ_1 is immediately re-oxidised, i.e. M_{red} is converted to M_{ox} ($t > 0$),

$$M_{red,1}\big|_{\Gamma_1} = 0, \quad (16)$$

$$D_{M_{ox,2},z} \left.\frac{\partial M_{ox,2}}{\partial z}\right|_{\Gamma_1} = D_{M_{ox,1},z} \left.\frac{\partial M_{ox,1}}{\partial z}\right|_{\Gamma_1} + D_{M_{red,1},z} \left.\frac{\partial M_{red,1}}{\partial z}\right|_{\Gamma_1},$$

$$M_{ox,1}\big|_{\Gamma_1} = M_{ox,2}\big|_{\Gamma_1}. \quad (17)$$

3.3 Initial conditions

The biosensor operation starts when the substrate S and the mediator M_{ox} are infused into the buffer solution ($t = 0$),

$$S_i = M_{ox,i} = 0, \quad (r, z) \in \overline{\Omega}_i \backslash \Gamma_4, \quad i = 1, 2, 3, 4, \quad (18)$$

$$S_4|_{\Gamma_4} = S_0, \quad M_{ox,4}\big|_{\Gamma_4} = M_0, \quad (19)$$

where S_0 and M_0 are the concentrations of the substrate and the mediator in the buffer solution.

Initially, the whole enzyme is in the oxidised form. We assume the homogeneous distribution of the enzyme in the enzyme layer ($t = 0$),

$$E_{ox,1} = E_0, \quad (r, z) \in \Omega_1,$$
$$E_{red,i} = 0, \quad (r, z) \in \Omega_i, \quad i = 1, 2;$$
$$M_{red,1} = 0, \quad (r, z) \in \Omega_1, \quad (20)$$

where E_0 stands for the initial concentration of the enzyme.

We also assume that the CNT mesh homogeneously saturates with the enzyme at a concentration possibly different from that in the enzyme layer,

$$E_{ox,2} = \eta E_0, \quad (r, z) \in \Omega_2, \quad t = 0, \quad (21)$$

where η is the ratio the enzyme initial concentration in the enzyme layer Ω_1 to that in the CNT layer Ω_2, practically, $0 \le \eta < 1$ [12].

3.4 Biosensor response

The response of the biosensor is generated due the electrochemical reaction (3). The electrons released in this reaction form a current that is amplified and presented to the end-user. The biosensor current is usually proportional to the area of the electrode surface [15,17]. When analyzing unit cells of the amperometric biosensor, the current is often normalised with the area of the base of the unit cell [19].

The electrochemical reaction (3) takes place in the layer of the enzyme-loaded CNTs. As the reaction is assumed to be very fast, its rate fully depends on the concentration of M_{red}, which is generated as a product of the reaction (2). Consequently, in the region Ω_2 the rate of the electrochemical reaction (3) is equal to the rate of the enzymatic reaction (2). Therefore, the current density $j_{\Omega_2}(t)$ generated in the enzyme-loaded CNT layer at time t is defined as

$$j_{\Omega_2}(t) = \frac{n_e F k_2}{\pi r_2^2} \int_0^{2\pi} \int_{z_1}^{z_2} \int_0^{r_2} E_{red,2} M_{ox,2} r \, dr \, dz \, d\varphi, \tag{22}$$

where n_e is a number of electrons released in the mediator re-oxidation, and F is the Faraday constant.

M_{red} is also generated in the enzyme layer (Ω_1). Differently from the region Ω_2, here the mediator is not re-oxidised. The M_{red} produced in Ω_1 is consumed on the boundary Γ_1. The density j_{Γ_1} of the current induced by the M_{red} in this layer can be explicitly obtained from the Faraday and Fick laws,

$$j_{\Gamma_1}(t) = -\frac{n_e F D_{M_{red,1},z}}{\pi r_2^2} \int_0^{2\pi} \int_0^{r_2} \left. \frac{\partial M_{red,1}}{\partial z} \right|_{\Gamma_1} r \, dr \, d\varphi. \tag{23}$$

The total current density is a sum of densities defined in (22) and (23),

$$\begin{aligned}
j(t) &= j_{\Omega_2}(t) + j_{\Gamma_1}(t) \\
&= \frac{2 n_e F}{r_2^2} \int_0^{r_2} \left(k_2 \int_{z_1}^{z_2} E_{red,2} M_{ox,2} dz - D_{M_{red,1},z} \left. \frac{\partial M_{red,1}}{\partial z} \right|_{\Gamma_1} \right) r \, dr.
\end{aligned} \tag{24}$$

For biosensors it is common to consider the current generated by the biosensor at the steady state conditions [1,2,18]. The current density for the considered biosensor at the steady state is defined as

$$J = \lim_{t \to \infty} j(t). \tag{25}$$

3.5 Effective diffusion coefficients

For the simplicity, the species S, M_{ox} and M_{red} are assumed to have the same diffusion properties, i.e. the diffusion coefficients of all these species are assumed to be the same for a certain medium.

The enzyme (Ω_1) and the Nernst (Ω_4) layers are assumed to be homogeneous,

$$
\begin{aligned}
D_{U_1,r} = D_{U_1,z} = D_e, \quad U_1 \in \{S_1, M_{ox,1}, M_{red,1}\}, \\
D_{U_4,r} = D_{U_4,z} = D_n, \quad U_4 \in \{S_4, M_{ox,4}\},
\end{aligned}
\tag{26}
$$

where D_n stands for the diffusion coefficient of the substrate and the mediator in the buffer solution as well as in the Nernst diffusion layer, and D_e is the corresponding diffusion coefficient in the enzyme. These diffusion coefficients are applied to all the space directions.

Due to a non-homogeneous distribution of the carbon nanotubes, the effective diffusion coefficients for the regions Ω_2 and Ω_3 can be obtained by applying the homogenization process [29,30].

The enzyme-loaded CNT composite layer (Ω_2) can be considered as a three compartment domain: the enzyme, the carbon nanotubes and the buffer solution. The holes of the perforated membrane (Ω_3) consist of two compartments: the carbon nanotubes and the buffer solution. The effective diffusion coefficients for these two mediums can be expressed in terms of the volume fraction, the tortuosity and the diffusion coefficients for the consisting compartments [29–32],

$$
\begin{aligned}
D_{U_2,\zeta} = \theta_{2,\zeta}(v_2 D_{CNT,U} + \eta_2 D_e + (1 - v_2 - \eta_2)D_n), \ U_2 \in \{S_2, M_{ox,2}\}, \\
D_{U_3,\zeta} = \theta_{3,\zeta}(v_3 D_{CNT,U} + (1 - v_3)D_n), \quad U_3 \in \{S_3, M_{ox,3}\}, \ \zeta \in \{r, z\},
\end{aligned}
\tag{27}
$$

where v_i and η_2 stand for the volume fractions of the CNTs and the enzyme, respectively, $0 < v_i, \eta_2 < 1$, $D_{CNT,U}$ is the diffusion coefficient of the species U in the carbon nanotubes, and $\theta_{i,r}$, $\theta_{i,z}$ are the tortuosities of the medium in r and z directions, respectively, $i = 2, 3$. Values of the tortuosities $\theta_{i,r}$ and $\theta_{i,z}$ depend on the structural anisotropy of the CNTs, particularly on the nanotubes orientation [29].

Assuming small values of the diffusion coefficient $D_{CNT,U}$ as well as of the volume fractions v_2, v_3 [33], the volume fraction η_2 approaches to η, and the expression (27) of the effective diffusions coefficients reduces to

$$
\begin{aligned}
D_{U_2,\zeta} = \theta_{2,\zeta}(\eta D_e + (1 - \eta)D_n), \quad U_2 \in \{S_2, M_{ox,2}\}, \\
D_{U_3,\zeta} = \theta_{3,\zeta} D_n, \quad U_3 \in \{S_3, M_{ox,3}\}, \quad \zeta \in \{r, z\},
\end{aligned}
\tag{28}
$$

where η is the ratio introduced in (21).

4 Numerical simulation

The mathematical model (7)–(25) of the biosensor has been defined as an initial boundary value problem based on a system of partial differential equations containing

non-linear terms representing biochemical reactions. Similar systems can be analytically solved only in very special cases [18,34]. Therefore, the problem (7)–(25) was solved numerically by applying the method of finite differences together with the method of alternating directions [23,24].

The domain of the model was discretised using a uniform grid individually for each region Ω_i, $i = 1, 2, 3, 4$. Each region was divided into 50 equal parts in the space directions r and z. A constant step $\tau = 10^{-4}$ s was used in the time direction.

The approximation was done applying semi-implicit finite difference schemes. The diffusion terms were approximated by the backward differences, while the reaction terms were approximated by the forward differences. The approximation resulted with a system of linear algebraic equations with a tri-diagonal matrix. Systems having tri-diagonal matrices are solved very effectively and therefore are advantageous for solving similar problems [23,24]. In this work the computer simulation was carried out using a software developed by the authors in C++ programming language [35].

In the simulation, the biosensor response time was assumed as the time when the change of the biosensor current over time remains very small during a relatively long term. A special dimensionless decay rate ϵ was used,

$$T_R = \min_{j(t)>0} \left\{ t : \frac{d\,j(t)}{d\,t} \times \frac{t}{j(t)} < \epsilon \right\}. \tag{29}$$

In this work we used $\epsilon = 10^{-2}$ for the calculations. The current density $j(T_R)$ was considered as a current density produced by the biosensor at a steady state.

When analyzing an influence of the geometry on the biosensor response, it is more convenient to operate with thicknesses of the layers instead of points z_i,

$$d_i = \begin{cases} z_1, & \text{for } i = 1, \\ z_i - z_{i-1}, & \text{for } i = 2, 3, 4, \end{cases} \tag{30}$$

where d_i is the thickness of i-th layer, $i = 1, 2, 3, 4$.

The following parameter values were used as a basic configuration of the biosensor [12,36]:

$$
\begin{aligned}
& r_1 = 2 \times 10^{-7}\text{m}, \quad r_2 = 8 \times 10^{-7}\text{m}, \\
& d_1 = 10^{-7}\text{m}, \quad d_2 = 4 \times 10^{-7}\text{m}, \quad d_3 = 10^{-5}\text{m}, \quad d_4 = 1.5 \times 10^{-4}\text{m}, \\
& \text{E}_0 = 4.55 \times 10^{-2}\text{mol m}^{-3}, \quad n_e = 2, \\
& D_e = 3 \times 10^{-10}\text{m}^2\text{s}^{-1}, \quad D_n = 2D_e = 6 \times 10^{-10}\text{m}^2\text{s}^{-1}, \\
& k_1 = 6.9 \times 10^2\text{m}^3\text{mol}^{-1}\text{s}^{-1}, \quad k_2 = 6.9 \times 10^4\text{m}^3\text{mol}^{-1}\text{s}^{-1}, \\
& \eta = 0.5, \quad \theta_{2,r} = \theta_{3,r} = \theta_r = 0.125, \quad \theta_{2,z} = \theta_{3,z} = \theta_z = 0.25.
\end{aligned} \tag{31}
$$

The proposed mathematical model (7)–(25) was validated by comparing the biosensor response obtained by using computer-aided experiments with the results of the corresponding physical experiments [12]. The experimental data along with the corresponding simulated data are depicted in Fig. 3.

Fig. 3 The dynamics of the biosensor current obtained experimentally (1, 3, 5) as well as modelled (2, 4, 6) at different concentrations of the mediator and the substrate: $M_0 = 0.2$, $S_0 = 9.9$ (1, 2), $M_0 = 0.05$, $S_0 = 4.98$ (3, 4), $M_0 = 0.005$, $S_0 = 1.99 \, \text{mol m}^{-3}$ (5, 6). Values of other parameters were defined in (31)
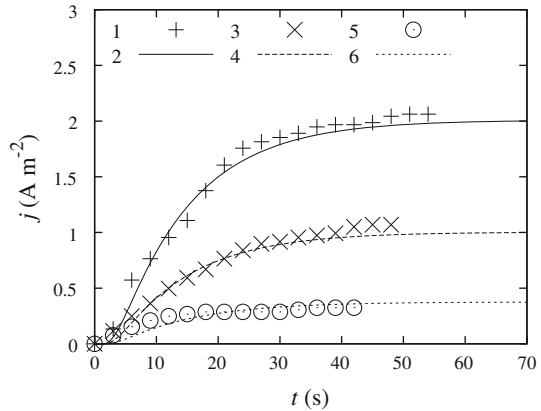
As one can see in Fig. 3, the simulation results are similar to the experimental data. In the cases presented in the figure the relative error of the simulation is less than 10% when the sensor approaches to the steady state. This error can be considered as small enough, referring to the fact that the results of repeated physical experiments can also vary about 10% [12].

5 Results and discussion

The behaviour of the biosensor response was investigated by using computer simulation. In order to investigate the influence of the model parameters on the response behaviour, the simulation was performed at wide ranges of the parameter values.

5.1 Effect of the structural anisotropy of the nanotubes

The mesh of carbon nanotubes influences the diffusivity of the species inside the composite medium containing the nanotubes. An experimental measurement of the diffusion coefficients is rather complicated [33].

The tortuosity is a characteristic of the CNT electrode mesh substantially influencing the effective diffusion coefficients (28). In terms of the biosensor structure, the tortuosity mainly depends on the anisotropy of the nanotubes inside the composite electrode. Two model parameters, θ_r and θ_z, stand for the directional anisotropy of the CNTs. Numerical experiments were employed in order to investigate the impact of the directional anisotropy on the biosensor response. Fig. 4 shows the dependence of the density of the steady state current on the tortuosity θ_z.

As one can see in Fig. 4, the impact of the diffusivity along the axis r on the response of the biosensor is relatively low. Fifty times increase of θ_r increases the response current less than 3% for all employed values of θ_z. The impact of θ_z, in comparison to θ_r, is much higher. In general, the directional anisotropy of the CNTs can result in a noticeable change of the steady state biosensor current. The sensitivity of the response to changes in θ_z can be explained by a relatively great thickness of the perforated

Fig. 4 Dependence of the biosensor response on the anisotropy of the CNT mesh. The density J of the stationary current versus the tortuosity θ_z was calculated at $S_0 = 10 \, \text{mol m}^{-3}$, $M_0 = 0.05 \, \text{mol m}^{-3}$ and two values of the radial tortuosity θ_r: 0.01 (1) and 0.5 (2). Values of other parameters are as defined in (31)
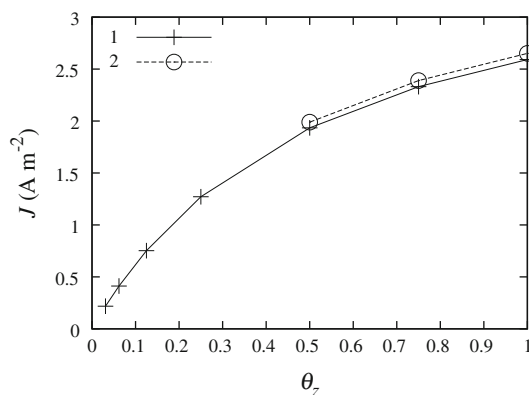
membrane. The membrane thickness d_3 is almost in two orders of magnitude greater than the radius r_1 of the membrane holes.

An insensibility of the biosensor response to changes in the tortuosity θ_r in the radial direction can be applied to further reduction of the mathematical model (7)–(25) to the corresponding one-dimensional-in-space mathematical model for the response simulation of biosensors having the structure as presented in Fig. 1. For much more efficient 1-D modelling, the perforated membrane can be approximated as proposed in [37].

5.2 Effect of the enzyme concentration

During the biosensor preparation, some enzyme penetrates into the mesh of the carbon nanotubes. The concentration of the enzyme filling the prepared CNT mesh can not be precisely determined because of the enzyme permanent inactivation and some other factors. Numerical simulation was employed in order to investigate the effect of the concentration of the enzyme in the CNT layer (region Ω_2). The concentration of the enzyme in this region was expressed as ηE_0, and therefore the biosensor response was simulated at different values of the parameter η. Figure 5 shows the simulated stationary biosensor current versus the substrate concentration S_0.

The initial concentration of the enzyme in the CNT layer has relatively low impact on the biosensor output at low concentrations of the substrate. At higher concentrations ($S_0 > 10 \, \text{mol m}^{-3}$), the influence of η on the response notably increases. At relatively low substrate concentrations the overall kinetics of the enzymatic reaction is usually of the first order while at high concentrations the kinetics is of the zero order [1,2,18,19]. So, the effect of η on the biosensor response is notably greater when the reaction kinetics is of the zero order rather than the kinetics is of the first order. A greater η corresponds to the higher enzyme concentration in the CNT layer. A higher enzyme concentration relates to a higher substrate concentration S_0 at which the reaction kinetics switches from the first to the zero order. The Michaelis constant well characterises the length of the biosensor calibration curve [1,2]. The apparent Michaelis constant $K_{M,app}$ is known to be the substrate concentration resulting in a half-maximum of the biosensor activity,

Fig. 5 The steady state biosensor current J versus the substrate concentration S_0 calculated at the mediator concentration $M_0 = 0.05 \, \text{mol m}^{-3}$ and three values of the filling degree η: 0 (1), 0.5 (2) and 1 (3), keeping all other parameters constant as defined in (31)
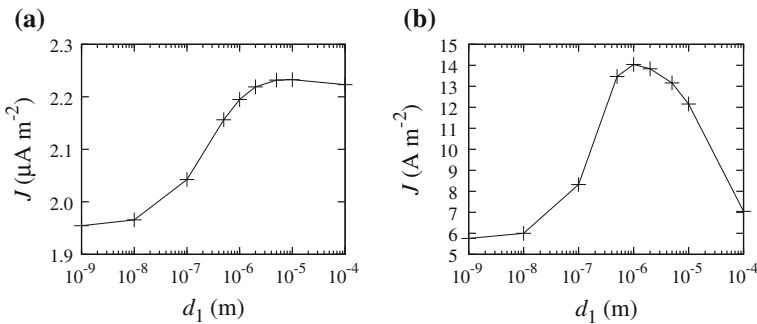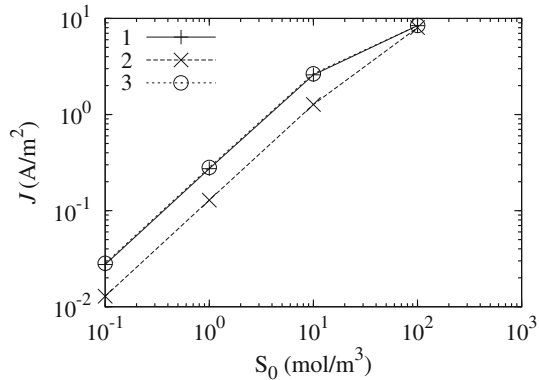
Fig. 6 The density J of the steady state current versus the thickness d_1 of the enzyme layer at the substrate concentration S_0 of 10^{-5} (a) and $100 \, \text{mol m}^{-3}$ (b). Values of other parameters are the same as in Fig. 5

$$K_{M,app} = \left\{ s : J(s) = 0.5 \lim_{S \to \infty} J(S) \right\}, \tag{32}$$

where $J(S)$ is the density of the stationary biosensor current calculated at the substrate concentration S, i.e. $S_0 = S$.

The dashed lines in Fig. 5 schematically show the $K_{M,app}$ values for the cases with $\eta = 0$ and $\eta = 1$. As one can see, the apparent Michaelis constant $K_{M,app}$ is about 3.5 times higher for the biosensor with the highly enzyme-loaded CNT layer (curve 3) than for the biosensor with no enzyme-loaded CNT layer (curve 1).

5.3 Effect of the thickness of the enzyme layer

The influence of the thickness d_1 of the enzyme layer (region Ω_1) on the biosensor response was investigated by simulating the steady state responses at very different values of d_1. The numerical experiments were repeated for two extremely different values of the substrate concentration S_0: $S_0 = 10^{-5}$ (Fig. 6a) and $100 \, \text{mol m}^{-3}$ (Fig. 6b).

Figure 6 shows a non-monotonous dependence of the steady state response on the thickness d_1 of the enzyme layer. The stationary biosensor current approaches to

non-zero value even at $d_1 = 0$. At zero thickness of the enzyme layer the enzymatic reactions (1) and (2) still take place in the enzyme-loaded CNT layer (region Ω_2).

The non-monotonous behaviour of the biosensor current is observed at all substrate concentrations used in the simulation. However, the thickness d_1 of the response peak depends on the concentration S_0 of the substrate. The maximal current is generated at $d_1 \approx 10^{-5}$ m for $S_0 = 10^{-5}$ mol m^{-3} and at $d_1 \approx 10^{-6}$ m for the substrate concentration $S_0 = 100$ mol m^{-3}. The stationary biosensor current also depends on the substrate concentration. In the case of low substrate concentration when $S_0 = 10^{-5}$ mol m^{-3}, the response peak is only about 15% higher than the response obtained at extremely thin enzyme layer ($d_1 = 10^{-9}$ m). For higher substrate concentrations, the impact of d_1 increases. In the case of $S_0 = 100$ mol m^{-3}, the corresponding difference in the response reaches even 140%. Similar non-monotonous dependence of the biosensor response on the thickness of the enzyme layer is also observed for the amperometric biosensors with solid electrodes [38], though the biosensors structures notably differ.

5.4 Effect of the perforation level of the membrane

The perforated membrane as the outer layer of the biosensor influences the behaviour of the device because of an additional diffusion limitation created to the substrate and the mediator. This section presents an investigation of the influence of the membrane perforation level on the behaviour of the biosensor response. The perforation level ρ is expressed as the ratio of the volume occupied by the holes to the overall volume of the membrane,

$$\rho = \frac{\pi r_1^2 d_3}{\pi r_2^2 d_3} = \frac{r_1^2}{r_2^2}, \quad 0 < \rho < 1. \tag{33}$$

To investigate the effect of the perforation level, the numerical simulations were performed at different substrate concentrations as well as different levels of the membrane perforation. The results of the investigation are presented in Fig. 7.

Fig. 7 The effect of the membrane perforation level ρ on the steady state biosensor current J. The experiments were performed using $S_0 = 0.1$ (1), 1 (2), 10 (3) and 100 mol m^{-3} (4). Other parameters were kept constant at values defined in (31) and $M_0 = 0.05$ mol m^{-3}
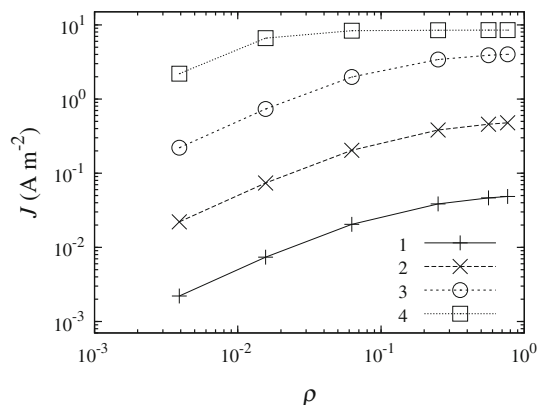
As one can see in Fig. 7, at relatively small values of the perforation level ($\rho < 0.01$) the stationary current is practically a linear increasing function of the level ρ, while at large values of ρ it is practically constant. However, this property is affected by the substrate concentration S_0. At higher concentration S_0 the biosensor response is less sensitive to changes in ρ than at lower one. When the analytical system becomes saturated with the substrate (curve 4) the biosensor current stagnates at a vide range of the level ρ.

The similarity of the shapes of curves (1), (2) and (3) in Fig. 7 means that the biosensor response is also proportional to the substrate concentration S_0. This proportionality is practically linear at low substrate concentrations (curves 1, 2 and 3). This effect is easily shown in Fig. 5.

The impact of the perforation of the outer membrane has been recently investigated for the amperometric biosensors with a solid electrode [22]. Although the structures of the solid and CNT electrodes are substantially different, our results are compatible with the results published in [22]. The main difference is in monotony of the biosensor response. In the case of the solid electrode the steady state biosensor current is a non-monotonous function of the perforation level [22], the corresponding function is monotonous in the case of CNT electrode (Fig. 7). However, the behaviour of the response of the CNT-based biosensor versus the perforation level is more similar to that of the amperometric plate-gap biosensor versus the permeability of the outer porous membrane [39]. Similarly to the CNT electrode and differently from the solid electrode, the electrochemical reaction in the case of the plate-gap electrode takes place not only at the basic (bottom) electrode surface but also on the walls.

6 Conclusions

The developed mathematical model (7)–(25) can be successfully used to simulate the behavior of the amperometric biosensors based on the carbon nanotubes deposited on the perforated membrane (Fig. 1). The model was validated by experimental data. The relative difference between the simulation results and experimental data was less than 10% at different concentrations of the substrate and the mediator (Fig. 3).

The numerical investigation showed that a change of the anisotropic properties of CNT can result in a notable change of the steady state biosensor current (Fig. 4). The steady-state current of the biosensor is a non-monotonous function of the thickness of the basic enzyme layer (Fig. 6) and a monotonous increasing function of the membrane perforation level (Fig. 7).

The sensitivity of the biosensors based on the CNT electrode can be increased by selecting an appropriate geometry of the biosensor. The computational simulation of the biosensor action can be used as a tool in design of novel highly sensitive biosensors based on nanoparticles.

References

1. F. Scheller, F. Schubert, *Biosensors* (Elsevier, Amsterdam, 1992)
2. A.P.F. Turner, I. Karube, G.S. Wilson, *Biosensors: Fundamentals and Applications* (Oxford University Press, Oxford, 1987)
3. B.D. Malhotra, A. Chaubey, Sens. Actuators, B **91**, 117 (2003)
4. U. Wollenberger, F. Lisdat, F.W. Scheller, *Frontiers in Biosensorics 2, Practical Applications* (Birkhauser Verlag, Basel, 1997)
5. D. Yu, B. Blankert, J.-C. Virè, J.-M. Kauffmann, Anal. Lett. **38**, 1687 (2005)
6. S. Iijima, Nature **354**, 56 (1991)
7. A.J.S. Ahammad, J.-J. Lee, M.A. Rahman, Sensors **9**, 2289 (2009)
8. K. Balasubramanian, M. Burghard, Anal. Bioanal. Chem. **385**, 452 (2006)
9. Y. Huang, H.G. Sudibya, D. Fu, R. Xue, X. Dong, L.-J. Li, P. Chen, Biosens. Bioelectron. **24**, 2716 (2009)
10. H.-J. Jiang, H. Yang, D. Akins, J. Electroanal. Chem. **623**, 181 (2008)
11. S. Wang, Q. Zhang, R. Wang, S. Yoona, Biochem. Biophys. Res. Commun. **311**, 572 (2003)
12. J. Razumienė, J. Gurevičienė, J. Barkauskas, V. Bukauskas , A. Šetkus, in *Biodevices 2009: Proceedings of the International Conference on Biomedical Electronics and Devices* (2009), pp. 448–452
13. C. Amatore, A. Oleinick, I. Svir, N. da Mota, L. Thouin, Nonlinear Anal. Model. Contr. **11**, 345 (2006)
14. I. Stamatin, C. Berlic, A. Vaseashta, Thin Solid Films **495**, 312 (2006)
15. L.D. Mell, T. Maloy, Anal. Chem. **47**, 299 (1975)
16. J. Kulys, Anal. Lett. **14**, 377 (1981)
17. P.N. Bartlett, R.G. Whitaker, J. Electroanal. Chem. **224**, 27 (1987)
18. T. Schulmeister, Sel. Elect. Rev. **12**, 203 (1990)
19. R. Baronas, F. Ivanauskas, J. Kulys, *Mathematical Modeling of Biosensors, Springer Series on Chemical Sensors and Biosensors, vol. 9* (Springer, Berlin, 2010)
20. M.E.G. Lyons, Int. J. Electrochem. Sci. **4**, 77 (2009)
21. M.E.G. Lyons, Int. J. Electrochem. Sci. **4**, 1196 (2009)
22. R. Baronas, J. Kulys, F. Ivanauskas, J. Math. Chem. **39**, 345 (2006)
23. D. Britz, *Digital Simulation in Electrochemistry, Lecture Notes in Physics, vol. 666*, 3rd edn. (Springer, Heidelberg, 2005)
24. A.A. Samarskii, *The Theory of Difference Schemes* (Marcel Dekker, New York-Basel, 2001)
25. C. Deslous, C. Gabrielli, M. Keddam, A. Khalil, R. Rosset, B. Trobollet, M. Zidoune, Electrochim. Acta **42**, 1219 (1997)
26. R. Baronas, F. Ivanauskas, A. Survila, J. Math. Chem. **27**, 267 (2000)
27. V. Levich, *Physicochemical Hydrodynamics* (Prentice Hall, Englewood Cliffs, 1962)
28. J.J. Gooding, A. Chou, J. Liu, D. Losic, J.G. Shapter, D.B. Hibbert, Electrochem. Commun. **9**, 1677 (2007)
29. S. Whitaker, *The Method of Volume Averaging, Theory and Applications of Transport in Porous Media, vol. 13* (Kluwer, Boston, 1999)
30. N. Bakhvalov, G. Panasenko, *Homogenisation: Averaging Processes in Periodic Media, Mathematics and its Applications, vol. 36* (Kluwer, Dordrecht, 1989)
31. R. Bertram, M. Pernarowski, Biophys. J. **74**, 1722 (1998)
32. D. Yankov, Enzyme Microb. Technol. **34**, 603 (2004)
33. M. Mu, N. Clarke, R.J. Composto, K.I. Winey, Macromolecules **42**, 7091 (2009)
34. M.E.G. Lyons, T. Bannon, G. Hinds, S. Rebouillat, Analyst **123**, 1947 (1998)
35. W.H. Press, S.A. Teukolsky, W.T. Vetterling, B.P. Flannery, *Numerical Recipes in C++: The Art of Scientific Computing*, 2nd edn. (Cambridge University Press, New York, 2002)
36. D.R. Lide (ed.), *CRC Handbook of Chemistry and Physics*, 85th edn. (CRC Press, New York, 2004)
37. K. Petrauskas, R. Baronas, Nonlinear Anal. Model. Contr. **14**, 85 (2009)
38. R. Baronas, F. Ivanauskas, J. Kulys, Sensors **3**, 248 (2003)
39. R. Baronas, F. Ivanauskas, I. Kaunietis, V. Laurinavicius, Sensors **6**, 727 (2006)